International Journal of Remote Sensing
Vol. 31, No. 14, 20 July 2010, 3885–3898

Taylor & Francis
Taylor & Francis Group

Evaluation of surface heat fluxes in Chiayi plain of Taiwan by remotely sensed data

TZU-YIN CHANG†, YUEI-AN LIOU*†, CHUAN-YAO LIN‡, SHAW-CHEN LIU‡ and YI-CHEN WANG§

†Center for Space and Remote Sensing Research, National Central University, 300 Jhongda Road, Jhongli City, Taoyuan, Taiwan, 32001, ROC

‡Research Center for Environmental Changes, Academia Sinica, 128 Academia Road, Nankang, Taipei, Taiwan, ROC

§Department of Geography, National University of Singapore, 1 Arts Link, 117570 Singapore

Surface energy processes have an essential role in regional weather, climate and hydrosphere cycles, as well in regulating urban heat redistribution. The Chiayi urban area of Taiwan and its surrounding agricultural plains are an appropriate complex for studying land surface parameters and energy fluxes of different land cover/land use types in an urban heat island. In this study, three micro-meteorological stations were established over Chiayi Plain to collect *in situ* reference observations from 2006. In order to properly characterize the surface heat fluxes over a regional scale by point measurement, Moderate Resolution Imaging Spectroradiometer (MODIS) satellite images and images acquired by a high resolution airborne campaign in conjunction with meteorological data were used to estimate the surface heat fluxes over a large area. The analytical results indicated that surface heat fluxes determined from both airborne and satellite images were feasible for estimating surface heat flux. The correlation coefficient of surface heat fluxes with *in situ* corresponding observations exceeded 0.80. On the other hand, satellite-observed surface skin temperature and land surface energy fluxes were the core factors analysed in different land cover types. The urban surface was rather dry as half of net radiation is converted to sensible heat flux for heating the surface, whereas over 90% net radiation is converted to latent heat flux at wet surfaces such as evergreen broadleaf or water. Surface heat flux was also proven to be an indicator of the magnitude of urban heat island effect and the findings of this study encouraged further use of remotely sensed imagery for assessing the urban heat island effect.

1. Introduction

The European heat wave in the summer of 2003 claimed thousands of lives. The strength of the heat wave was enhanced by the heat island effect in central business districts (CBDs) and residential areas. Urban areas have a large number of man-made structures and constructions such as buildings and roads, primarily made of asphalt and concrete. The man-made structures have changed not only the land surface characteristics and energy balance by influencing the surface albedo, thermal capacity and heat conduction, but also the landscape by increasing the surface roughness, thus reducing the rate of ventilation in urban areas (Nichol 1998, Anandakumar 1999, Pena 2008). Moreover, preferential heating of the city over the surrounding area

*Corresponding author. Email: yueian@csrsr.ncu.edu.tw

International Journal of Remote Sensing
ISSN 0143-1161 print/ISSN 1366-5901 online
http://www.tandf.co.uk/journals
DOI: 10.1080/01431161.2010.483481

increased convection over the city, which then trapped the heat inside the urban area. Because evapotranspiration or latent heat by plants are major cooling processes on the surface and in the atmosphere, replacing forested areas with buildings and roads may reduce this cooling effect in urban areas. This is most likely the major cause of the urban heat island effect (Cotton and Pielke 1996, Giorgi *et al.* 1999).

Over the last four decades Taiwan has achieved extremely rapid economic development, leading to a ~20-fold increase in energy usage. Since only less than one third of the country is characterized as flat land, the highly developed industry and densely populated areas have meant that the Western Plain of Taiwan is now covered in large numbers of cities, small towns, factories and roads. Finally, Taiwan not only has severe known environmental problems, but many areas of the country are now affected by the urban heat island phenomenon.

Studying the heat island effect requires understanding of the roles of land surface parameters, including evapotranspiration and surface heat fluxes. Previous studies have proposed methods of estimating surface flux, such as the eddy covariance system, the Bowen ration system, and empirical methods such as soil water balance. However, these methods, which rely on point observations, cannot effectively address the spatial variability of the surface energy (Courault *et al.* 2005). With the development of remote sensing technology, varied data such as high spatial resolution airborne images and high temporal resolution satellite images are now available for retrieving spatially-distributed surface heat fluxes (Norman *et al.* 1995, Bastiaanssen *et al.* 1998, Schumugge *et al.* 1998, Granger 2000, French *et al.* 2003, 2005, McCabe and Wood 2006). In addition, most operational approaches for estimating surface heat flux by remote sensing use the energy balance concept, and methods such as the Surface Energy Balance Algorithm for Land (SEBAL; Bastiaanssen *et al.* 1998), the Surface Energy Balance System (SEBS; Su 2002), the Simplified Surface Energy Balance Index (S-SEBI; Roerink *et al.*, 2000) and resistance–surface energy balance (RSEB; Kalma and Jupp 1990) have been developed and applied to evapotranspiration or surface heat flux estimation in different land cover types.

The remote sensing data mainly provide surface parameters such as surface albedo, vegetation index and surface temperature for surface heat flux estimation in energy balance models. Cleugh *et al.* (2007) indicated that, when estimating the surface heat flux by energy balance models, the surface temperature obtained from remote sensing thermal bands is a problematic issue because an energy-balance constraint of the sensible flux estimation derived from the surface skin temperature is not easy to set. Therefore, redistribution for sensible and latent heat fluxes using scatter plots of surface albedo versus temperature is proposed to solve the problem in this study. Moreover, prior studies have also addressed the influence of different land covers on sensible heat flux and surface temperature (Nemani and Running 1997, Mildrexler *et al.* 2006, 2007). Kato and Yamaguchi (2007) also addressed the value of ground heat flux over the urban area. This study aims to analyse the impacts of different land cover types on surface energy partitioning processes.

2. Observational requirements

2.1 *Energy flux model*

The proposed methodology for measuring surface heat fluxes from remotely sensed data and auxiliary data is based on the theory of surface energy and radiation balance. The surface energy balance at the land–air interface can be written as equation (1),

and the net radiation is considered a residual radiation from soil heat flux, sensible heat flux and latent heat flux.

$$R_n = G_0 + (H) + (LH), \tag{1}$$

where R_n is the net radiation (W m^{-2}), G_0 is the soil heat flux (W m^{-2}), H is the sensible heat flux (W m^{-2}), and LH is the latent heat flux (W m^{-2})

Given stable atmospheric conditions, the surface radiation balance and surface energy balance can be combined to estimate surface heat flux. Net radiation is first derived by the radiation balance, which can be expressed as equation (2), and the net radiation can be derived as a physical and practical equation written as equation (3).

$$R_n = R_s^{\downarrow} - R_s^{\uparrow} + R_L^{\uparrow} - R_L^{\downarrow} \tag{2}$$

$$R_n = R(1-\alpha)R_s^{\downarrow} + R_L^{\uparrow} - \varepsilon_0 \sigma T_0^4, \tag{3}$$

where R_n is the net radiation, and incoming shortwave radiation $R_s^{\downarrow}$ is assumed constant for the imaging time. The emitted shortwave radiation $R_s^{\uparrow}$ is defined by surface albedo $(\alpha)R_s^{\downarrow}$, the emitted longwave radiation $R_L^{\uparrow}$ is defined by the Stefan Boltzmann equation depending on surface temperature (T_0), and the incoming longwave radiation $R_L^{\downarrow}$ is derived from an empirical formula applied by Wukelic *et al.* (1989).

Soil heat flux (G_0), which is determined by the thermal conductivity of the soil and the temperature gradient of the topsoil, can be derived using the method developed by Kustas and Daughtry (1990) and Bastiaanssen *et al.* (1998) which is a function of surface albedo, surface temperature, and normalized difference vegetation index (NDVI) written as:

$$G_0 = R_n T_0 (0.0038 + 0.0074\alpha)(1 - 0.98(\mathrm{NDVI})^4), \tag{4}$$

where the normalized difference vegetation index, NDVI, is defined as a ratio of the difference in reflectivities of the near-infrared and red band to their sum:

$$\mathrm{NDVI} = \frac{\rho_{\mathrm{NIR}} - \rho_{\mathrm{RED}}}{\rho_{\mathrm{NIR}} + \rho_{\mathrm{RED}}} \tag{5}$$

The sensible heat flux (H) is the rate of heat loss, due to the temperature difference between two heights. However, the stability of atmospheric conditions needs to be considered to calculate sensible heat flux. In this study, atmospheric stability is analysed using a numerical iteration method in which the Monin–Obukhov length is considered as a convergence threshold, and the stability corrections for momentum and heat transport are computed using the Dyer (1974) formula. The sensible heat flux can be calculated using equation (6):

$$H = \frac{u^* \kappa \rho_{air} C_p (T_0 - T_a)}{\left[\mathrm{In}\left(\frac{z_2 - z_d}{z_1 - z_d}\right) - \left(\Psi_h\left(\frac{z_2 - z_d}{L}\right) + \Psi_h\left(\frac{z_1 - z_d}{L}\right)\right)\right]} \tag{6}$$

$$u^* = \frac{u_r \kappa}{\left[\left(\frac{\mathrm{In} z_r}{z_0}\right) - \Psi_m\right]} \tag{7}$$

$$L = \frac{-u_*^3 \rho_{\text{air}}}{kg\left(\frac{(\text{H})}{T_a C_p} + \frac{0.61(\text{LH})}{\lambda_v}\right)}, \tag{8}$$

where κ is the von Karman's constant (= 0.4), u^* is the friction velocity (m s^{-2}) computed as in equation (7), ρ_{air} is air density (kg m^{-3}), C_p is the air specific heat (= 1004 J(kg K^{-1})$^{-1}$), L is the Monin–Obukhov length computed as in equation (8), g is the gravitational constant (= 9.81 m s^{-2}), z_0 is the aerodynamic resistance (m), u_r is the wind speed at height z_r (m s^{-2}), z_d is the displacement height (m), and Ψ_h and Ψ_m are the stability corrections for heat and momentum transport, respectively. The value T_0 is the surface temperature (K), and T_a is the air temperature (K).

After the iterative process, the latent heat flux can be estimated as a residual item in equation (1). However, remotely sensed data usually include numerous pixels or areas such as very dry regions; thus, heat fluxes in some regions are often over- or under-estimated. Therefore, the fraction factor (Λ) is derived from the scattering plot of surface albedo versus temperature (figure 1) (Roerink *et al.*, 2000). Then the regional latent heat and sensible heat fluxes from the imagery can be estimated as follows:

$$(\text{LH})_f = \Lambda(\text{LH}) \tag{9}$$

$$\text{H}_f = R_n - G_0 - (\text{LH})_f, \tag{10}$$

where LH and H are the latent heat and sensible heat fluxes after the iteration process, respectively; and $(\text{LH})_f$ and H_f are the latent heat and sensible heat fluxes after the above redistribution correction process, respectively.

2.2 *Study area*

Figure 2 shows the study area, which is located at 23.3–23.6°N latitude and 120.1–120.6°E longitude and includes a total area of about 1600 km^2. Some eastern areas of the study area are hill landforms, and most areas are flat plain. The climate of the study area is classified as subtropical monsoon. Precipitation in Chiayi Plain differs by location and year. Of the average annual rainfall of 2000 mm, about 85% occurs in the rainy season. The average temperature is 23.3°C. The highest and lowest temperatures occur in July and January, respectively. Due to its climate and topography, Chiayi Plain is a major agricultural region in Taiwan.

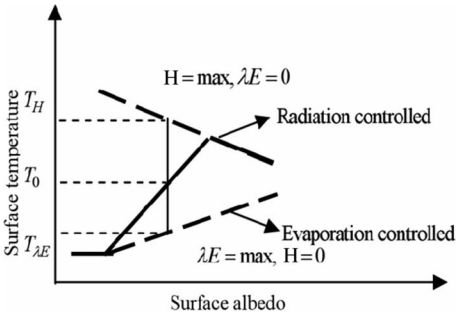

Figure 1. A schematic diagram showing the relation between surface albedo and temperature (Liou *et al.* 2002).

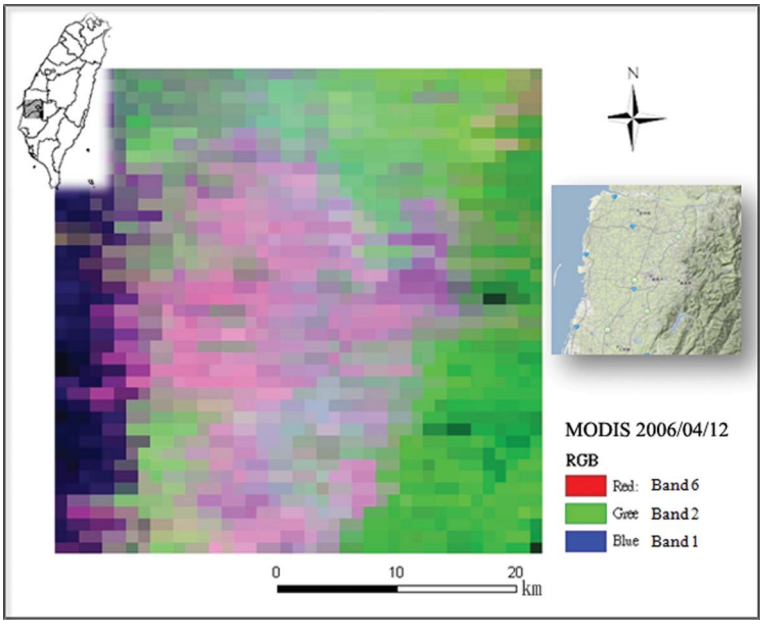

Figure 2. False-colour image showing the area of interest, Chiayi Plain, taken on 12 April 2006, and composed of photographs obtained at three bands of Terra MODIS: Band 1 (blue), Band 2 (green) and Band 6 (red).

2.3 *Data collection*

Three micro-meteorological stations have been established in Chiayi Plain since 2006. They include an eddy covariance system (Chiayi Girl's Senior High School, 23° 28' 23.72"N, 120° 26' 58.99"E) and two Bowen ratio systems (Niaoxiu Station, 23° 29′ 27.78″ N, 120° 24′ 26.20″ E, and Guogou Station, 23° 29′ 58.33″ N, 120° 20′ 06.02″ E). The eddy covariance system is located in an urban area with concrete surface, and the two Bowen ratio systems were installed in the crop fields. These stations acquire surface meteorological data and incoming and outgoing radiance at minute frequent intervals. The data are used as a reference for remote sensing analysis and as a main evidence for calculating the magnitude of the Chiayi area heat island effect.

Due to the high resolution 8 m FORMASAT-2 images without thermal bands and to test the feasibility of using remote sensing technology to retrieve the regional surface heat fluxes over Chiayi plain in Taiwan, an airborne campaign was performed. On 27 December 2006, airborne thermal infrared data was acquired using a FLIR (Forward Looking Infrared) system with a ThermoVision® A40M thermal infrared camera. The camera was mounted on a helicopter and used to obtain a thermal infrared spectrum from 7.5 to 11 μm. For this particular mission, the data were collected at several altitudes, which resulted in a varied spatial resolutions ranging from 0.8 m to 1 m. In this study, the multispectral FORMOSAT-2 image taken on 1 January 2007 was combined with the airborne thermal images as a high resolution dataset to derive surface parameters such as surface albedo (α), NDVI and surface temperature (T_0) for estimating regional surface heat fluxes from remotely sensed data. On the other hand, another key objective was to evaluate the feasibility of long-term monitoring for the surface heat fluxes over Chiayi plain using relatively

Table 1. Details of the FORMOSAT-2 and MODIS bands used in this study

Band	Bandwidth (μm)	Spectral region
FORMOSAT-2 (Spatial resolution: 8 m)		
1	0.45–0.52	Blue
2	0.52–0.60	Green
3	0.63–0.69	Red
4	0.76–0.90	Near infrared (NIR)
MODIS (Spatial resolution: 1 km)		
1	0.620–0.670	Red
2	0.841–0.876	Near infrared (NIR)
3	0.459–0.479	Blue
4	0.545–0.565	Green
31	10.78–11.28	Thermal infrared (TIR)
32	11.77–12.27	Thermal infrared (TIR)

low-resolution satellite images. Moderate Resolution Imaging Spectroradiometer (MODIS) is a scientific payload launched onboard the Terra and Aqua satellites by National Aeronautics and Space Administration (NASA) in 1999 and 2002, respectively. The instruments record data for 36 spectral bands ranging from 0.4 μm to 14.4 μm and at varying spatial resolutions: 250 m for bands 1–2, 500 m for bands 3–7 and 1 km for bands 8–36. Therefore, several cloud-free MODIS Level 1B onboard Terra images in 2006 acquired from Center for Space and Remote Sensing Research (CSRSR), National Central University in Taiwan were used to achieve the purposes.

Table 1 shows the FORMOSAT-2 and MODIS bands used in this study. Four MODIS bands including blue, green, red and near-infrared bands were aggregated to 1 km resolution to derive the surface broadband albedo; the surface albedo is estimated as following regression which was built by Liou *et al.* (2008) for the Chiayi area:

$$\alpha = 1.0488r_{\text{blue}} + 1.1779r_{\text{green}} + 0.31132r_{\text{red}} - 0.65569r_{\text{NIR}}, \tag{11}$$

where r_{blue}, r_{green}, r_{red} and r_{NIR} are reflectivity in the blue, green, red and near-infrared (NIR) bands, respectively.

MODIS bands 31 and 32 were used to retrieve surface skin temperature (T_s) which is adapted from the following equation from Pawan (2004):

$$T_s = 0.39(T_{31})^2 + 2.34T_{31} - 0.78T_{31}T_{32} - 1.34T_{32} + 0.39(T_{32})^2 + 0.56, \tag{12}$$

where T_{31} and T_{32} are the brightness temperature of MODIS bands 31 and 32, respectively.

3. Results

3.1 *Spatially-distributed surface energy fluxes*

Before analysing the airborne thermal infrared images, a georectification procedure was required since the images were not associated with a coordinate system, because the flight engineering data lacked sufficient precision for registering onto the images. As a result, the image-to-image registration that used 0.5 m digital orthophotos from Council of Agriculture, Executive Yuan as reference was used to georectify the airborne images. The first order polynomial function and the nearest neighbour

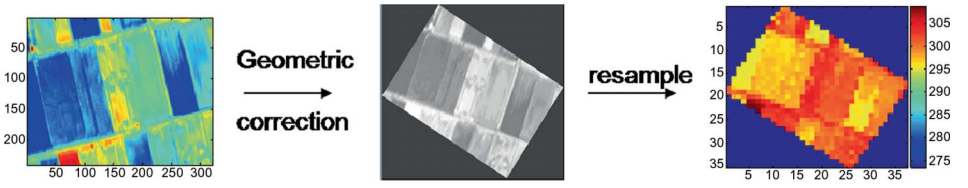

Figure 3. Flowchart of airborne image processing.

resampling method was used to resample the image to FORMOSAT-2 resolution (8 m), and the total rms for these registrations was less than 0.3 m. Figure 3 shows the georectification process.

Due to a miscommunication, only Guogou Station was in the flight path of the 27 December 2006 mission, as no other airborne images was available at other two stations. Therefore, the following discussion of the imaging results refers to data for Guogou Station. Table 2 compares instantaneous surface energy fluxes retrieved from the airborne image and *in situ* data. The heat fluxes retrieved from the airborne image are close to the *in situ* measurements, which demonstrated the feasibility of using remote sensing data to calculate surface heat flux.

Figure 4 presents the instantaneous surface heat fluxes, the net radiation (R_n), soil heat flux (G_0), sensible heat flux (H), and latent heat flux (LH) retrieved from the airborne image. The land in this area is mainly cropland. Figure 4 shows that crop types are easily distinguishable by surface heat flux. The rice paddy (350 W m^{-2}) revealed a higher latent heat flux than the corn field (250 W m^{-2}) did, but the sensible heat flux was inversely related. Further, the net radiation over corn was higher than that over rice paddy, and soil heat flux of corn was lower than that of rice paddy. These characteristics resulted from different environmental path radiances and plant structures.

However, the satellite image does have a disadvantage in terms of spatial resolution. Its advantages include the frequent revisiting schedule and low image cost, unlike airborne systems, which are subject to weather conditions, air space restriction, and high operational cost. Therefore, MODIS images are selected to study the performance of coarse resolution image for estimating surface heat fluxes. Figure 5 shows a comparison of the instantaneous sensible and latent heat fluxes retrieved from 12 MODIS images and the *in situ* measurement from Niaoxiu Station. The correlation coefficient of surface heat fluxes with *in situ* measurement is 0.85, and the mean biases of the sensible heat flux and latent heat flux are 67.12 W m^{-2} and 129.75 W m^{-2}, respectively. Several prior studies have interpreted the reason why the mean biases of sensible heat and latent heat fluxes are so high. The energy imbalance is addressed in ground flux measurements

Table 2. Comparison of the instantaneous surface heat fluxes retrieved from airborne image with the *in situ* measurements.

	R_n (W m^{-2})	G_0 (W m^{-2})	H (W m^{-2})	LH (W m^{-2})
Retrieved data	343.96	39.55	10.56	289.52
Guogou Station	424.45	13.33	24.66	386.48

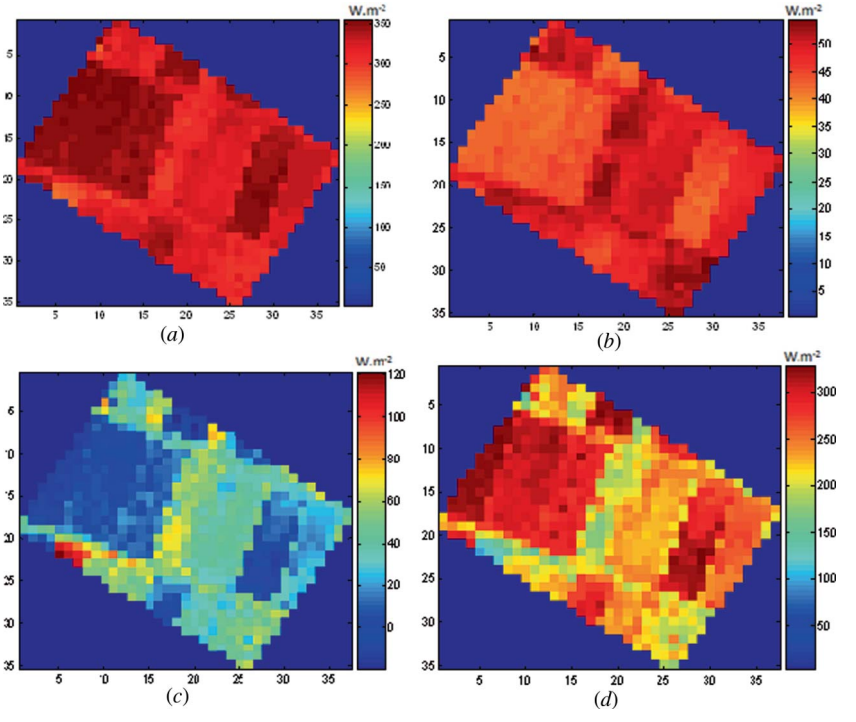

Figure 4. Instantaneous distributions of (*a*) net radiation (R_n); (*b*) soil heat flux (G_0); (*c*) sensible heat flux (H); and (*d*) latent heat flux (LH) estimated from combining airborne and FORMOSAT-2 datasets. The image is from 27 December 2006. The dark blue areas indicate no value.

using eddy covariance systems which often underestimate the sensible and latent heat fluxes. The studies indicate that the underestimation is about 20% and it could be as high as 50% or even greater if the technique is not applied properly (Twine *et al.* 2000, Lee *et al.* 2004). On the other hand, for ground flux measurements, Bowen ratio systems often underestimate or overestimate the sensible and latent heat fluxes because the energy budget is a forced closure assumption in these methods (Baldocchi *et al.* 2001, Wilson and Goldstein 2002).

3.2 *Surface energy fluxes over different land cover*

These results indicate that regional surface heat fluxes are properly determined from both airborne and satellite images. According to the energy budget concept, when the surface is wet or heavily vegetated, net energy is mainly consumed by evaporation and evapotranspiration of water in soil and vegetation. In other words, most net radiation is converted to latent heat flux. However, when the surface is rather dry, little of the latent heat flux is consumed, and most net radiation is converted to sensible heat flux for heating the surface. Urban surfaces covered with asphalt and concrete are rather dry as most net radiation is converted to sensible heat flux for heating the surface. As for the areas of wet surface, latent heat flux may play a role in cooling the surface temperature. Therefore, analysing surface energy fluxes associated with changes in land cover and land use types in the study area is essential. The land cover

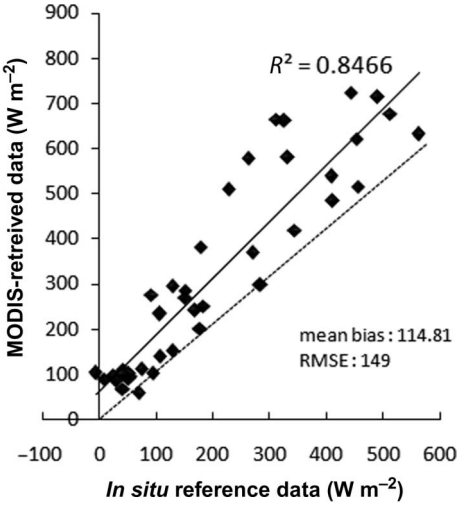

Figure 5. Relationship of instantaneous sensible and latent heat fluxes between MODIS-retrieved and *in situ* data.

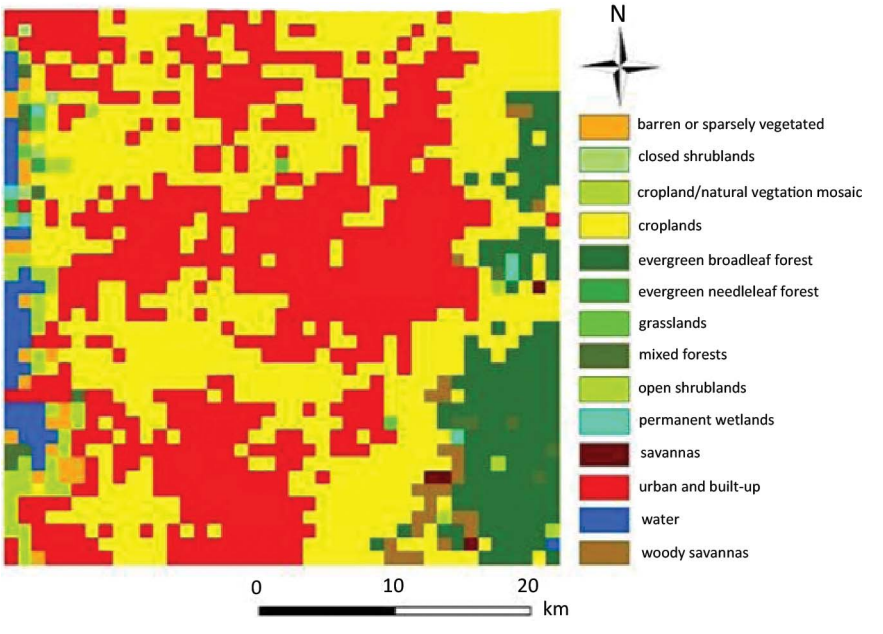

Figure 6. Land cover classification of Chiayi area.

classification image used in this study is the 2004 MODIS land cover MOD12Q14 (MODIS/Terra Land Cover Type Yearly L3 Global 1 km SIN Grid V004) product from the Land Processes Distributed Active Archive Center (LPDAAC) of the US Geological Survey website. Figure 6 shows that the primary land cover scheme identifies 17 classes of land cover defined by the International Geosphere-Biosphere

Programme (IGBP). The forest areas appear in dark green, cropland is in yellow, and the urban and built-up areas are in red.

A total of 30 MODIS Level 1B images acquired in 2006 were used to estimate the surface heat fluxes over the study area. The monthly average surface temperature and surface heat fluxes were derived for comparison with different kinds of land cover types. Figure 7 shows that surface temperature of urban surface is highest in all kinds of land cover, and figure 8 shows the monthly average surface heat fluxes over four different land cover types. The net radiation of the evergreen broadleaf surface is highest because the albedo of evergreen forest is usually lower than other types. However, the possible reasons for underestimated net radiation over water surface could be due to its low coverage of only 2.2% in the study area, and most fish farms here classified as water surface. The value range of soil heat flux in different types is only about 25 W m^{-2}. Equation (4) can be improved in soil heat flux estimation of an urban area. Compared with the sensible heat flux and latent heat flux in different land cover types, the results indicate that the urban surface is rather dry, as half of net radiation is converted to sensible heat flux for heating the surface, and croplands transfer about 36% of the net radiation energy into sensible heat fluxes and 64 % into the latent heat fluxes. The water surface and evergreen broadleaf surface are converted to latent heat flux (96% and 93%, respectively). This indicates that water in soil and vegetation is consumed by evaporation and evapotranspiration. However, it is found that the trends of croplands in surface temperature and surface heat fluxes are similar to urban and built-up surfaces. This may be due to the cropland that is usually near urban areas; the spectrum curve is similar to that of the built-up surface, causing the classification errors in lower resolution images such as MODIS data.

Finally, figure 9 compares the average surface temperature with average sensible heat and latent heat fluxes of different land cover types. This study indicated that the correlation coefficient of sensible heat and latent heat fluxes with surface temperature are about 0.97 and 0.79, respectively. The relationship between the surface heat flux such as sensible heat and latent heat and temperature rise is a strong positive correlation, and surface heat flux can be used to quantify the urban heat island effect in the future study.

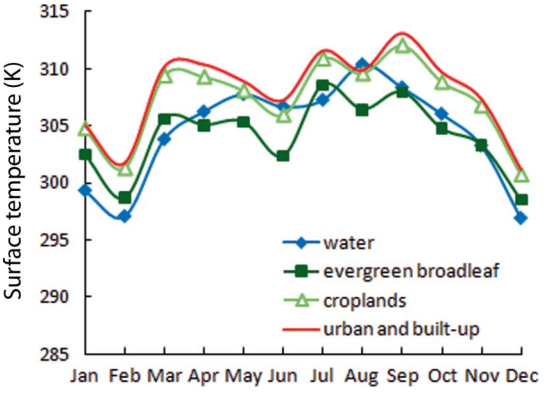

Figure 7. Monthly average surface skin temperature over different land covers.

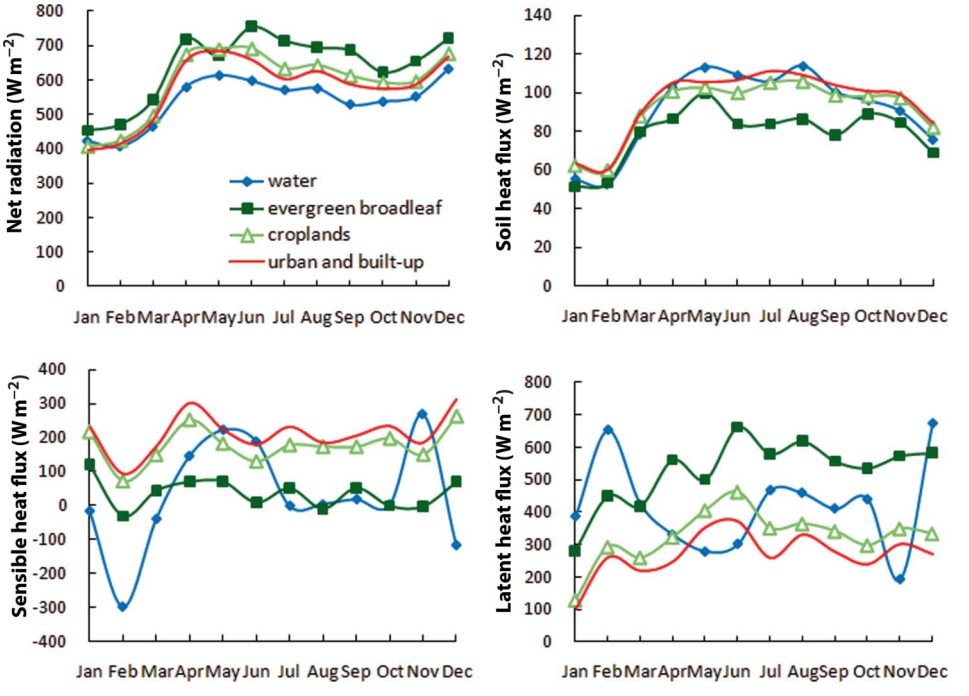

Figure 8. Monthly average surface heat fluxes over different land covers.

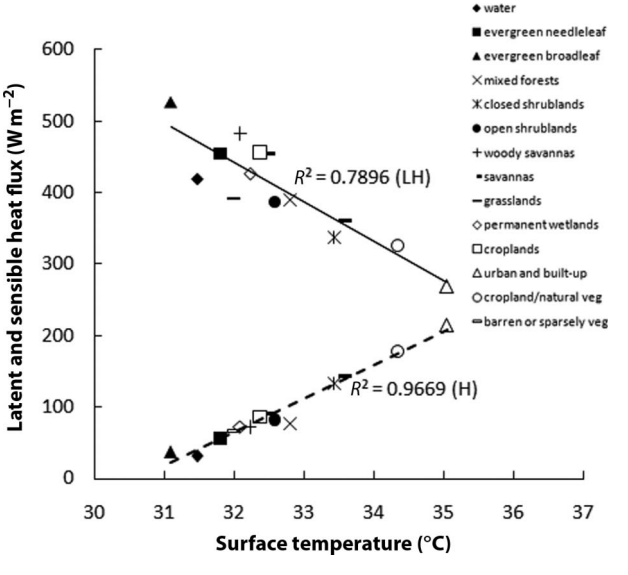

Figure 9. Relationship of sensible heat and latent heat and surface temperature for different land cover types.

4. Conclusion

Three methods, including traditional ground measurement, high-resolution airborne thermal sensing, and satellite-based remote sensing, are used in this study to estimate surface heat fluxes. According to the results, the remote sensing technique is an effective method to evaluate surface heat flux. Although airborne images can reveal detailed energy flux information, obtaining high-quality and high-quantity airborne images is difficult due to weather, labour, cost and restriction from regulations. On the other hand, satellite-based thermal sensing can provide a larger quantity of data. For example, the combination of Aqua and Terra satellites can provide up to four images per day, and the correlation coefficient of surface heat fluxes retrieved from MODIS data with *in situ* measurements is above 0.80 in this study. However, further work is needed to refine the analysis by using the MODIS data to retrieve surface energy such as the problems associated with geometry and radiometry. The problems can be resolved and further improved by careful calculation or implementation of proper geospatial techniques, and the authors expect to address these issues in future work.

In addition, MODIS satellite-observed surface skin temperature and land surface energy fluxes are core indicators for analysing land cover types. The analytical results indicate that half of net radiation is converted to sensible heat flux for heating the surface of urban and built-up surfaces. The cropland canopy such as rice paddy and sugar cane transfers about 36% of the net radiation energy into sensible heat flux and 64% into the latent heat flux. In wet surface areas such as evergreen broadleaf or water, over 90% net radiation is converted to latent heat flux. Finally, the results showed that increasing the wet surface area can effectively reduce the temperature rising. Furthermore, sensible heat flux can be considered as an indicator of the strength of urban heat island effect, and can be used to quantify the magnitude of the urban heat island effect in the future.

Acknowledgements

The authors would like to thank the Academic Sinica and National Science Council of Taiwan, Republic of China for partially financial support of this research (AS-93-TP-A04). They also appreciate the very constructive comments and patience of the reviewers in improving the manuscript.

References

Anandakumar, K., 1999, A study on the partition of net radiation into heat fluxes on a dry asphalt surface. *Atmospheric Environment*, **33**, pp. 3911–3918.

Baldocchi, D., Falge, E., Gu, L., Olson, R., Hollinger, D., Running, S., Anthoni, P., Bernhofer, C., Kenneth, D., Evans, R., Fuentes, J., Goldstein, A., Katul, G., Law, B., Lee, X., Malhi, Y., Meyers, T., Munger, W., Oechel, W., Paw, U.K.T., Pilegaard, K., Schmid, H.P., Valentini, R., Verma, S., Vesala, T., Wilson, K. and Wofsy, S., 2001, FLUXNET: A new tool to study the temporal and spatial variability of ecosystem-scale carbon dioxide, water vapor, and energy flux densities. *Bulletin of the American Meteorological Society*, **82**, pp. 2415–2434.

Bastiaanssen, W.G.M., Menenti, M., Feddes, R.A. and Holtslag, A.A.M., 1998, A remote sensing surface energy balance algorithm for land (SEBAL) 1. Formulation. *Journal of Hydrology*, **212–213**, pp. 198–212.

Cleugh, H.A., Leuning, L., Mu, Q. and Running, S.W., 2007, Regional evaporation estimates from flux tower and MODIS satellite data. *Remote Sensing of Environment*, **106**, pp. 285–304.

COTTON, W.R. and PIELKE, R.A., 1996, *Human Impacts on Weather and Climate*. (Cambridge, UK: Cambridge University Press).

COURAULT, D., SEGUIN, B. and OLIOSO, A., 2005, Review on estimation of evapotranspiration from remote sensing data: From empirical to numerical modeling approaches. *Irrigation and Drainage Systems*, **19**, pp. 223–249.

DYER, A.J., 1974, A review of flux–profile relationships. *Boundary-Layer Meteorology*, **7**, pp. 363–372.

FRENCH, A.N., SCHMUGGE, T.J., KUSTAS, W.P., BRUBAKER, K.L. and PRUEGER, J., 2003, Surface energy fluxes over El Reno, Oklahoma, using high-resolution remotely sensed data. *Water Resources Research*, **39**, pp. 1164.

FRENCH, A.N., JACOB, F., ANDERSON, M.C., KUSTAS, W.P., TIMMERMANS, W., GIESKE, A., SU, Z., SU, H., MCCABE, M.F., LI, F., PRUEGER, J. and BRUNSELL, N., 2005, Surface energy fluxes with the advanced spaceborne thermal emission and reflection radiometer (ASTER) at the Iowa 2002 SMACEX site (USA). *Remote Sensing of Environment*, **99**, pp. 55–65.

GIORGI, F., HUANG, Y., NISHIZAWA, K. and FU, C., 1999, Seasonal cycle simulation over eastern Asia and its sensitivity to radiative transfer and surface processes. *Journal of Geophysical Research*, **104**, pp. 6403–6424.

GRANGER, R.J., 2000, Satellite-derived estimates evapotranspiration in the Gediz basin. *Journal of Hydrology*, **229**, pp. 70–76.

KALMA, J.D. and JUPP, D.L.B., 1990, Estimating evaporation from pasture using infrared thermometry: Evaluation of a one-layer resistance model. *Agricultural and Forest Meteorology*, **51**, pp. 223–246.

KATO, S. and YAMAGUCHI, Y., 2007, Estimation of storage heat flux in an urban area using ASTER data. *Remote Sensing of Environment*, **110**, pp. 1–17.

KUSTAS, W.P. and DAUGHTRY, C.S.T., 1990, Estimation of the soil heat flux/net radiation ratio from spectral data. *Agriculture and Forest Meteorology*, **49**, pp. 205–223.

LEE, X., MASSMAN, W.J. and LAW, B., 2004, *Handbook of Micrometeorology: A Guide for Surface Flux Measurement and Analysis* (Dordrecht: Kluwer Academic Publishers).

LIOU, Y.-A., CHUANG, Y.-C. and LEE, T., 2002, Estimate of evapotranspiration over rice fields using high resolution DMSV imagery data. *Cross-Strait Symposium on the Remote Sensing and Agricultural Biotechnology*, 22–25 February, 2002, Chiayi, Taiwan, pp. 40–41.

LIOU, Y.-A., CHANG, T.-Y. and HO, H.-J., 2008, Estimation of evapotranspiration by using MODIS imagery over Chiayi Plain in Taiwan. *Cross-Strait Remote Sensing Workshop*, 15–19 September 2008, Guilin, China, pp. 100–110 (Beijing, China: Institute of Remote Sensing Applications, Chinese Academy of Sciences).

MCCABE, M.F. and WOOD, E.F., 2006, Scale influences on the remote estimation of evapotranspiration using multiple satellite sensors. *Remote Sensing of Environment*, **105**, pp. 271–285.

MILDREXLER, D., ZHAO, M. and RUNNING, S.W., 2006, Where are the hottest spots on Earth? *Eos, Transactions, American Geophysical Union*, **87**, pp. 461–467.

MILDREXLER, D., ZHAO, M., HEINSCH, F.A. and RUNNING, S.W., 2007, A new satellite-based methodology for continental-scale disturbance detection. *Ecological Applications*, **17**, pp. 235–250.

NEMANI, R.R. and RUNNING, S.W., 1997, Land cover characterization using multitemporal red, near-IR, and thermal-IR data from NOAA/AVHRR. *Ecological Applications*, **7**, pp. 79–90.

NICHOL, J.E., 1998, Visualization of urban surface temperatures derived from satellite images. *International Journal of Remote Sensing*, **19**, pp. 1639–1649.

NORMAN, J.M., KUSTAS, W.P. and HUMES, K.S., 1995, Two sources approach for estimating soil and vegetation energy fluxes in observations of directional radiometric surface temperature. *Agricultural and Forest Meteorology*, **77**, pp. 263–293.

PAWAN, K.S., 2004, Diagnosing irrigation water resources with multi-sensor remote sensing and GIS techniques– a case study of the Roxo Dam irrigation system. MSc thesis, International Institute for Geo-Information Science and Earth Observation, Enschede.

PENA, M.A., 2008, Relationships between remotely sensed surface parameters associated with the urban heat sink formation in Santiago, Chile. *International Journal of Remote Sensing*, **29**, pp. 4385–4404.

ROERINK, G.J., SU, Z. and MENETI, M., 2000, S-SEBI: A simple remote sensing algorithm to estimate the surface balance. *Advances in Space Research*, **25**, pp. 147–157.

SCHUMUGGE, T.J., KUSTAS, W.P. and HUMES, K.S., 1998, Monitoring land surface fluxes using ASTER observations. *IEEE Transactions on Geoscience and Remote Sensing*, **36**, pp. 1421–1430.

SU, Z., 2002, The surface energy balance system (SEBS) for estimation of turbulent heat fluxes. *Hydrology and Earth System Sciences*, **6**, pp. 85–99.

TWINE, T.E., KUSTAS, W.P., NORMAN, J.M., COOK, D.R., HOUSER, P.R. and MEYERS, T.P., 2000, Correcting eddy-covariance flux underestimates over a grassland. *Agricultural and Forest Meteorology*, **103**, pp. 279–300.

WILSON, K. and GOLDSTEIN, A., 2002, Energy balance closure at FLUXNET sites. *Agricultural and Forest Meteorology*, **113**, pp. 223–243.

WUKELIC, G.E., GIBBONS, D.E., MARTUCCI, L.M. and FOOTE, H.P., 1989, Radiometric calibration of LANDSAT Thematic Mapper thermal band. *Remote Sensing of Environment*, **28**, pp. 339–347.